Lasers in Surgery and Medicine 20:319–331 (1997)

Innate Cellular Fluorescence Reflects Alterations in Cellular Proliferation

Jian Chun Zhang, MD,[1] Howard E. Savage, PhD,[1] Peter G. Sacks, PhD,[1] Thomas Delohery, PhD,[2] R.R. Alfano, PhD,[3] A. Katz, PhD,[3] and Stimson P. Schantz, MD[1]

[1]Head and Neck Laboratory, Memorial Sloan-Kettering Cancer Center, New York, NY
[2]Flow Cytometry Core Faculty, Memorial Sloan-Kettering Cancer Center, New York, NY 10021
[3]NYS Center for Advanced Technology and Mediphotonic Laboratory, Physics Department, The City College of the City University of New York, New York, NY 10031

Background and Objective: **The objective of this study was to examine the question of whether unique spectral patterns were associated with cell proliferation and could be identified by comparing the fluorescence pattern of slow to rapid growing cells.**
Study Design/Materials and Methods: **Three in vitro model systems, (A431 cells inhibited by EGF, serum-starved 3T3 fibroblasts, and normal oral epithelial cells exposed to TGFβ), were analyzed using fluorescence spectroscopy. Growth status was monitored by cell number, ^{3}H-thymidine incorporation, and flow cytometry.**
Results: **The excitation spectra (λex 240–430 nm, λem 450 nm) effectively distinguished slow and rapid growing cells in all three systems. Statistical analysis of the ratios of the main broad peak (320–350 nm) to a point on the down-slope of the curve at 370 nm was statistically significant. Ratios in the emission scan (λex 340 nm, λem 360–660 nm) could separate slow and rapid growing A431 and oral epithelial cells (P=0.0001 and P=0.023, respectively), but not slow and fast growing 3T3 cells (P=0.56).**
Conclusion: **Innate cellular fluorescence has the potential to discriminate proliferating and nonproliferating cell populations. Lasers Surg. Medicine 20:319–331, 1997.** **© 1997 Wiley-Liss, Inc.**

Key words: biomarkers; cellular fluorescence; cell proliferation; flow cytometry

INTRODUCTION

Innate cellular and tissue fluorescence has been investigated as a novel diagnostic tool for the identification of preneoplastic and neoplastic tissue. Its relevance to clinical oncology may be manyfold including use as an intermediate endpoint biomarker in cancer chemoprevention trials [1]. Starting in 1984 in animals [2] and in 1987 in human tissue [3], different organ systems have been investigated both in vivo and in vitro using this technology including the lung [4], colon [5–8], skin [9], heart [10], breast [11], ovary [12], and cervix [13]. The fluorescence patterns of single cells have also been studied [14]. The underlying physical basis for such investigations is that fluorescence is strongly influenced by molecules found within cells and tissues and include flavins, aromatic amino acids, nicotinamide adenine dinucleotide (NADH), collagen and others, all of which fluoresce in the ultraviolet and visible regions of the light spectrum [15,16]. Tissues in varying stages of progression towards malignancy should differ from normal tissues in both the qualitative and quantitative nature of these

Contract grant sponsor: NIH; Contract grant number: CA29502; Contract grant sponsor: NASA, Contract grant number:49547-C.

*Correspondence to: Stimson P. Schantz, M.D., Head and Neck Service, Memorial Sloan-Kettering Cancer Center, 1275 York Avenue, New York, NY 10021.

Accepted for publication 26 April 1996.

© 1997 Wiley-Liss, Inc.

intrinsic cellular fluorophores. The examination of the fluorescence characteristics of such intrinsic cellular and tissue fluorophores has provided information about tissue microstructure and the changes therein without interfering with the native cellular environment [6,7,17].

Multiple excitation sources have been utilized in the detection of native cellular fluorescence, including argon [2,11], krypton [2], helium-cadmium [2,3,8,9], and pulsed-nitrogen lasers [5,6,7,13]. The instrumentation used in this study is a xenon lamp-based fluorescence spectrometer, CD-scan (Mediscience Technology, Cherry Hill, NJ). With this instrument, both excitation and emission spectra can be obtained from cell and tissue samples. Using this fluorescence spectrometer design and current bio-optical technology, the applicability of tissue autofluorescence analysis has been previously tested with two model systems. In an N-nitroso-N-methyl-benzylamine (NMBA)-induced rat esophageal cancer model, alteration of the (λex 220–360 nm, λem 380 nm) excitation spectrum correlated with disease progression from normal mucosa through dysplasia to invasive cancer [17]. In a multicellular tumor spheroid model, trans-retinoic acid (RA) altered autofluorescence profiles as assessed with multiple wavelengths including the excitation scans (λex 220–360 nm, λem 380 nm), (λex 260–430 nm, λem 450 nm), and the emission scans (λex 300 nm, λem 320–580 nm), (λex 340 nm, λem 360–660 nm) [18]. Such RA-induced alterations corresponded to changes in the state of spheroid differentiation [19,20]. In vivo human studies are in progress which suggest that neoplastic tissues within the upper aerodigestive tract can be discriminated from normal mucosa by their autofluorescence profile. Increased proliferation is well recognized as one of the fundamental biological changes in carcinogenesis [21]. Markers of cellular proliferation are often used as biomarkers in chemoprevention studies [22,23].

The purpose of this study was to identify the spectral signatures associated with cellular proliferation. The ability to detect such signatures would provide a basis for in vivo human investigations which examine mucosal proliferation profiles as a precursor to invasive disease, as well as a marker of response to chemopreventive agents. Proliferation and fluorescence data is presented on three in vitro model systems in which cellular proliferation was modulated. A431 cells, a human epidermoid carcinoma, were growth inhibited by EGF exposure [24]. Swiss 3T3 fibroblasts, a mouse embryo cell, were growth inhibited by serum-starvation [25]. Normal human oral epithelial cells were in primary culture and growth inhibited by TGFβ exposure [26].

MATERIALS AND METHODS

Cell Culture

Three cell types were used for experimentation. The human epidermoid carcinoma cell line A431 and a murine Swiss 3T3 fibroblast cell line (American Type Culture Collection, Rockville, MD, CCL 92), were maintained in log-phase culture in a 1:1 mixture of Dulbecco's modified Eagle medium and Ham's F12 (DMEM-F12) supplemented with fetal calf serum (FCS) (Gibco BRL, Grand Island, NY) and gentamicin (50 μg/ml). Mucosa was obtained from pediatric patients undergoing routine tonsillectomy. Normal human oral epithelial cells were derived from mucosa of the anterior tonsillar pillar using explant outgrowth techniques. Explants and oral epithelial cells were maintained in Aminomax-c100 medium (Gibco BRL). Primary epithelial outgrowths were used for all experiments. Growth was modulated and experiments performed in all three systems following 3 days of experimental manipulation. Cell seeding concentrations were empirically determined, as described in text, so as to insure that following 3 days of treatment, control cells would be in log phase. A431 cells were growth inhibited by treatment with 100 ng/ml EGF (Collaborative Research Inc., Bedford, MA) following 24 hours of attachment. 3T3 fibroblasts were growth inhibited by serum starvation. Oral epithelial cells were growth inhibited with 1 ng/ml TGFβ (R&D Systems, Minneapolis, MN).

Cell Proliferation Assays

Cell counting. Cell suspensions were made from monolayer cell cultures by trypsinization with a 0.125% trypsin-2 mM EDTA solution. The digestive activity of the trypsin was arrested by the addition of complete media. A431 and 3T3 cells were enumerated on a ZM Coulter Counter (Coulter, Hialeah, FL) and normal oral epithelial cells with a hemocytometer. Cell viability of control and treated cells was assessed using trypan blue dye exclusion and was routinely >95%.

H-thymidine incorporation. After 3 days of treatment, cells were pulsed with 2 μci/ml ^{3}H-thymidine (20 Ci/mmol, NEN Research Products, Boston, MA) for 2 hours 37°C. Monolayer cells were precipitated with trichloroacetic acid (TCA)

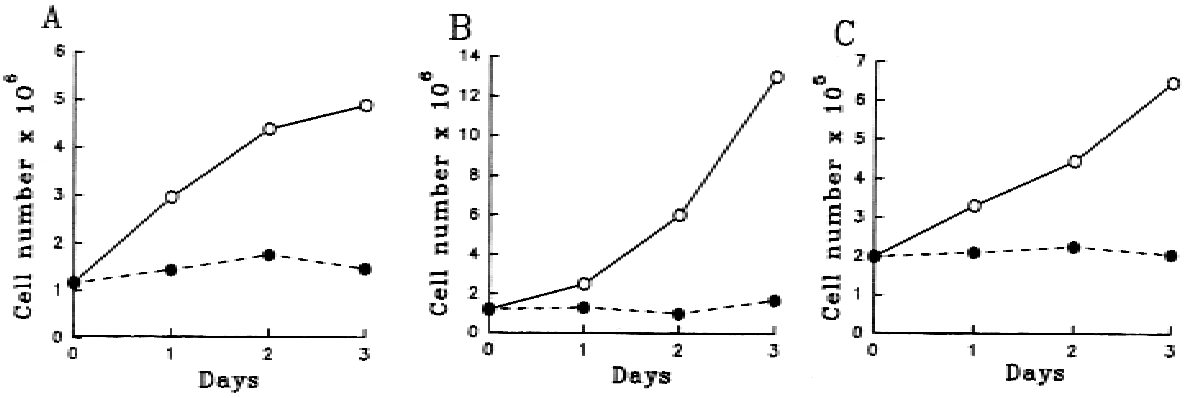

Fig. 1. Effects of growth inhibiting conditions are shown for A431 cells (**A**), 3T3 cells (**B**), and oral mucosal cells (**C**). The experimental and control cells of each respective cell type were plated and treated as described in the Materials and Methods section. Inhibitory manipulations started on day 0. A: A431 cells treated with (closed circles) or without (open circles) 100 ng/ml EGF; B: 3T3 cells treated with 10% FCS serum (open circles) or serum-free medium (closed circles); C: normal oral mucosal cells treated with (closed circles) or without (open circles), 1 ng/ml TGFβ.

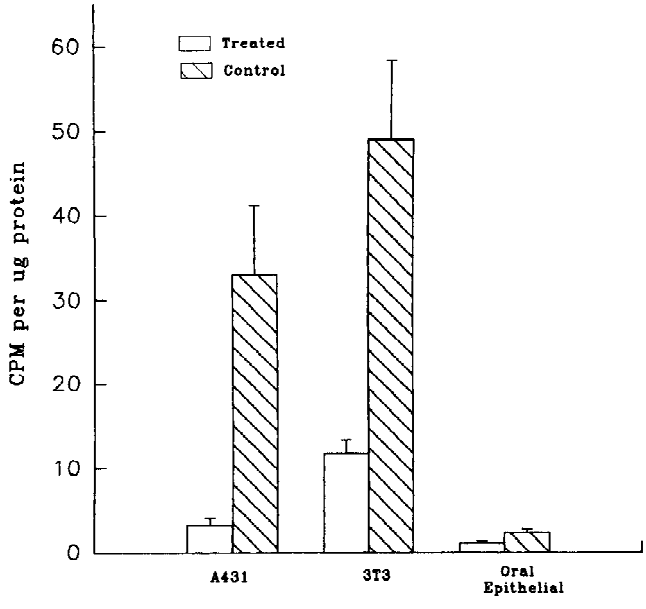

Fig. 2. Effects of growth inhibiting conditions on DNA synthesis were examined after 3 days of treatment. Cells were grown in control or experimental conditions for 3 days, pulsed for 2 hours with 2 μci/ml ^{3}H-thymidine, DNA precipitated with 5% TCA, and scintillation counted as described in Materials and Methods. A431 cells were treated with 100 ng/ml EGF, 3T3 cell were treated under serum-free conditions, and normal oral mucosal cells were treated with 1 ng/ml TGFβ as described in Figure 1. Treated cells are the open bars, control cells are the hatched bars. A431 ($N = 6$, $P = 0.013$); 3T3 ($N = 9$, $P = 0.0025$); oral epithelial ($N = 11$, $P = 0.0031$).

and then solubilized with 1N NaOH. An aliquot of the solubilized cells was saved for protein determination. TCA was then added to the solution of solubilized cells. The resultant precipitate was collected on a filter, washed with TCA and then ethanol, and dried for scintillation counting. Protein was determined by Bio-Rad assay (Bio-Rad, Melville, NY). Data is expressed as cpm/μg protein.

Flow cytometry. Cells were trypsinized as above, pelleted and fixed in 70% ethanol. Cellular DNA was stained with 50 μg/ml chromomycin A3 (CA3; Sigma Chemical Company, St. Louis, MO) in 100 mM $MgCl_2$. All data acquisition was performed on a FACStar Plus flow cytometer equipped with Consort 32 computer system running Lysys II software (Becton Dickinson, San Jose, CA). An argon laser tuned to 458 nm was used to excite the chromomycin A3 and for light scatter measurements. Small and large cell populations were resolved on the basis of scattered laser light. All DNA histograms used for cell cycle analysis were gated using pulse-processing electronics and software to eliminate debris and cell clumps. DNA histograms were analyzed using Multicycle software (Phoenix Flow Systems, San Diego, CA).

Fluorescence Analysis

Sample preparation. Three to 4 × 10^6 cells were trypsinized as above, pelleted, and a fibrin clot prepared as described [27]. The fibrin clot was used to achieve a stable cell pellet that could be physically moved and also to minimize the number of cells required for scanning. The cell pellet typically had a size of 3mm × 3mm × 10mm which was sufficient to cover the beam size of 2mm × 8 mm. The cell pellet was mixed with 20 μl fibrin (20 mg/ml concentration) and 10 μl thrombin (20 unit/ml concentration), and incu-

TABLE 1. Emission and Excitation Scans Performed on Each Sample

Emission scans[a]		Excitation scans[b]	
Excitation wavelength	Emission wavelength interval	Emission wavelength	Excitation wavelength interval
300 nm	320–580 nm	340 nm	200–320 nm
320 nm	340–620 nm	380 nm	200–360 nm
340 nm	360–660 nm	450 nm	240–430 nm
365 nm	400–700 nm	480 nm	250–460 nm
420 nm	440–800 nm	520 nm	270–500 nm
488 nm	500–800 nm		

[a]An emission scan is defined as the use of a single wavelength to excite tissue while a range of wavelengths emitted from the same tissue is analyzed for relative intensity.
[b]An excitation scan is defined as exciting tissue sequentially with a range of specific wavelengths and then recording the relative intensity of light emitted at a single wavelength.

bated in 5% CO_2 in air at 37°C for 20 minutes to ensure clot formation. For scanning, the clot was placed on the side of a quartz micro cuvette (NSG Precision Cells, Inc., Farmingdale, NY). The cuvette was placed in the scanner with the clot facing the excitation beam. All samples were scanned within 2 hours of clot formation. For scanning packed cells, approximately 15×10^6 cells were transferred into a quartz micro cuvette and repelleted in a microcentrifuge for several seconds to pack the cells and remove air bubbles. Photo bleaching was not observed in that rescanning the samples did not result in any spectral profile changes.

Fluorescence scanning. Cell clots were scanned with a CD Scanner (Mediscience Technology Corp.) which is a modified LS50B Perkin Elmer fluorescence spectrophotometer. Six emission scans and five excitation scans were measured (Table 1). The fluorescent spectrometer corrects emission spectra for spectral sensitivity of the detection optics by using its own internal software correction, based on a known rhodamine standard. Spectra are corrected for variations in the excitation intensity using a dual beam operation, where a ratio is made of the emission signal and a portion of the excitation beam. Detector dark current is eliminated by gating the photo multiplier tube at twice the pulse rate of the xenon lamp. The maximum spectral resolution of the excitation line and detection system with minimum slits is 2.5 nm. The maximum power density used over the experimental excitation range was in the order of 3–6 micro watts with a fluence of approximately 15–20 mJ/cm^2. The integration time is 0.06 seconds per data point. These scans were chosen because of their relationship to the major cellular and tissue fluorophores [28]. Selected scan intervals and appropriate cut off filters were used to eliminated back scattered light. For emission scans (λex 340 nm, λem 360–660 nm), a 350 nm long pass filter was positioned in the emission monochrometer to block scattered excitation light. For excitation scans (λex 240–430 nm, λem 450 nm), a 290 nm long pass filter was placed in the emission monochrometer, blocking excitation light below 290nm. The 290 nm filter was used since these scans had a lot of back scattered light at the lower wavelengths. For sake of comparisons, the scans were normalized to the major broad peak.

To control for the influence of time and the effect of the fibrin clot, control and growth inhibited 3T3 cell clots, as well as acellular clots, were scanned at 0, 2, 4, 6, 8, and 23 hours. The samples were maintained at room temperature during this period. Fluorescence analysis demonstrated that the fibrin clot alone emitted at 290 nm and did not influence cellular fluorescence at the points used for the ratio determinations (data not shown). The influence of time on the fluorescence of cell containing clots was negligible for the time periods analyzed (data not shown). For experimental analyses, all cells and clots were scanned within 2 hours of suspension.

RESULTS

Modulation of Cell Growth

To establish a model for comparison between proliferating and nonproliferating cells, the effects of modulating media conditions were initially examined (Fig. 1). Cell growth was reproducibly inhibited in the three in vitro cell systems tested. A431 epidermoid cells were inhibited by

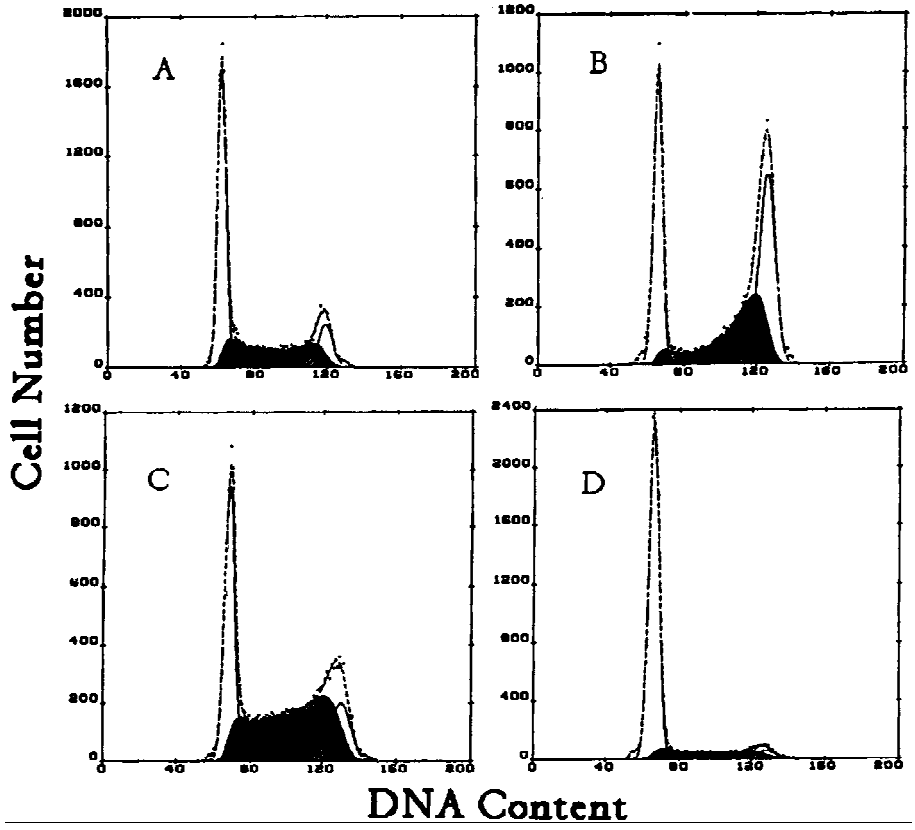

Fig. 3. Cell cycle distributions and size distributions are shown for 3 day control vs. growth inhibited cells. **A:** A431 cells grown in media; **B:** A431 grown in media with 100ng/ml EGF; **C:** 3T3 cells grown in 10% FCS; **D:** 3T3 cells grown in serum-free medium. Dotted line shows experimental values, solid lines show gaussean fit, and shaded areas represent S-phase.

culturing in the presence of 100 ng/ml EGF (Fig. 1A), 3T3 cells by growing in serum-free medium (Fig. 1B), and normal oral epithelial cells by addition of 1 ng/ml TGFβ (Fig. 1C). As shown in Figure 1, cell growth was inhibited in each cell system within 24 hours as determined by cell counts. By 3 days of culture, there was a minimum threefold difference in cell numbers between control and experimental cultures. Cell viability, as determined by trypan blue exclusion, was greater than 95% for each group. Based on the shape of the growth curves in Figure 1, subsequent studies were plated to ensure that 3-day control cultures would be in log phase. A431 and 3T3 cells were plated at 8.0×10^5 cells/100 mm Petri dish for control and 1.6×10^6 for experimental, and normal oral cells at 2.0×10^5 cells/60 mm dish.

To further characterize the proliferation status of the experimental and control cultures, cells were pulsed with ^{3}H-thymidine. As shown in Figure 2, DNA synthesis was decreased under all experimental conditions as reflected by a decrease in ^{3}H-thymidine incorporation.

Lastly, the proliferative status was analyzed using standard flow cytometric techniques (Figs. 3, 4). Following 3 days of experimental treatments, DNA was stained with CA3 and the fraction of cells within each phase of the cell cycle determined. Flow cytometric analysis of A431 cells (Table 2) indicated that there was an EGF-induced decrease in the G0/G1 population and an increase in G2/M, whereas the percent S-phase cells remained unchanged. Pictorial analysis (Fig. 3A,B) showed an accumulation of A431 cells in late S-phase indicative of an EGF-induced block in late S-G2/M phases. 3T3 fibroblasts under serum-free conditions showed an accumulation of cells in G0/G1 with concomitant decrease in both S and G2/M phases (Table 2) in accord with an induction of a G0/G1 block (Fig. 3C,D). The cell cycle distributions for normal epithelial cells were more complex in that a small cell population defined by region (R1) and a large cell population defined by

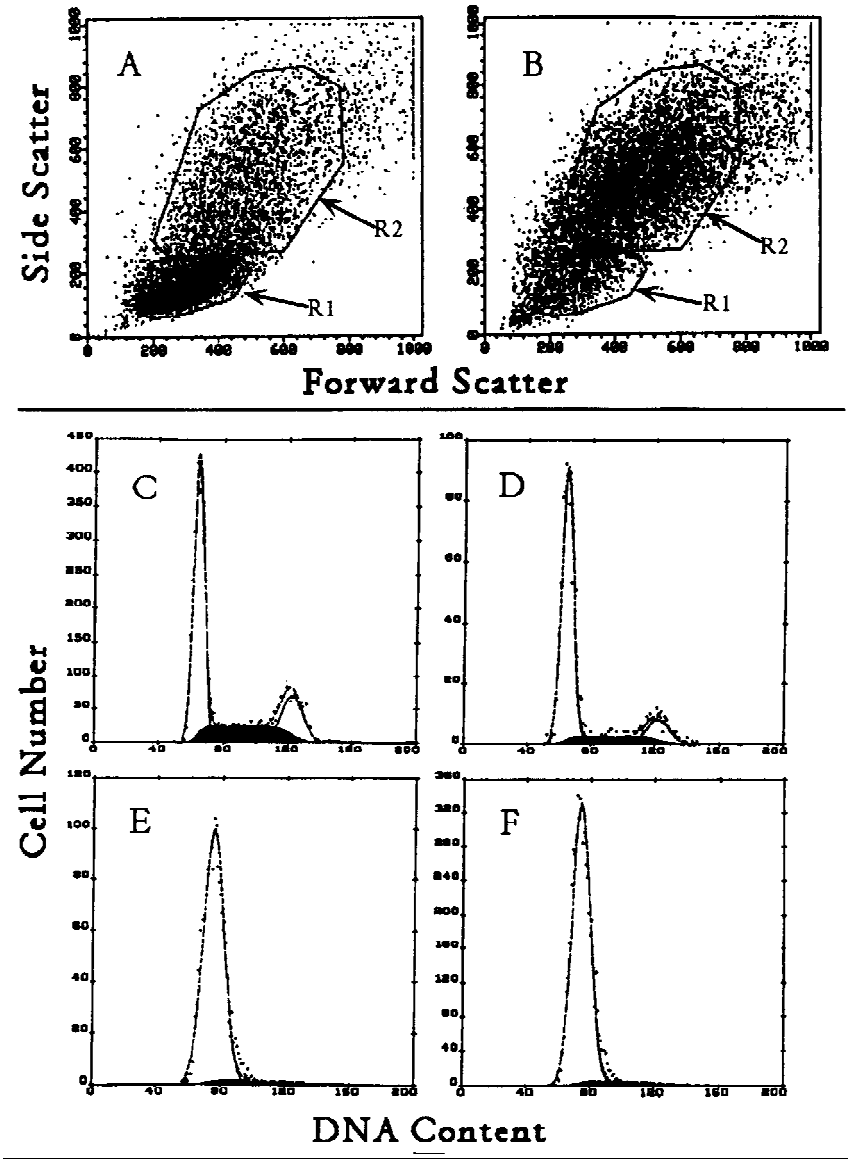

Fig. 4. Cell cycle distributions and size distributions for normal oral epithelial cells are shown for 3 day control vs. growth inhibited cells. **A:** Scatter measurements of normal oral epithelial cells growing in Aminomax-c100 medium; **B:** scatter measurements of normal oral epithelial cells growing in Aminomax-c100 medium plus 1 ng/ml TGFβ; **C:** cell cycledistributions of small control cells, region R1, from A; **D:** cell cycle distributions of small TGFβ treated cells, region R1, from B; **E:** cell cycle distributions of large control cells, region R2, from A; **F:** cell cycle distributions of large TGFβ treated cells, region R2, from B.

region (R2) were observed in each of the samples (Fig. 4A,B). The small R1 cells have a cell cycle distribution consisting of definitive G0/G1, S, and G2/M phases (Fig. 4C,D, Table 2). In contrast, the large R2 cells only show a broad G0/G1 peak with negligible cells in S phase (Fig. 4E,F, Table 2). Data in Figure 4 shows a representative experiment but does not give information on the percentage of large and small cells in each group. Following TGFβ treatment, there was a reproducible increase in the percentage of large cells. In Figure 4, the percentage of large cells in G0/G1 phase increased from 31 to 73% with TGFβ treatment. In seven individual experiments, the mean percentage of large cells increased from 42 to 68%. Morphologically, both control and TGFβ-induced large cells appear similar. They have an increased cytoplasmic to nuclear area ratio, but not the thin flattened appearance associated with terminally differentiated squames.

TABLE 2. Cell Cycle Distributions of 3 Day Control and Growth Inhibited Cells*

Cell line	Media[a]	Status[b]	Cell cycle distribution[c] %G0/G1	%S	%G2/M
A431	–	P	45 ± 2.09	41 ± 1.04	14 ± 1.73
A431	+	NP	38 ± 2.70	42 ± 2.00	20 ± 2.85
3T3	+	P	57 ± 12.6	30 ± 8.52	13 ± 4.14
3T3	–	NP	82 ± 2.93	14 ± 2.08	4 ± 0.99
Oral cells (S)	–	P	61 ± 3.45	22 ± 2.20	17 ± 2.03
Oral cells (S)	+	NP	66 ± 3.18	21 ± 2.60	16 ± 2.69
Oral cells (L)	–	P	94 ± 1.16	6 ± 1.16	ND[d]
Oral cells (L)	+	NP	96 ± 0.79	4 ± 0.79	ND

*Three day control and treated cells were trypsinized, fixed in ethanol, and stained with chromomycin A3.
[a]Media additives for A431, ± 100 ng/ml EGF; 3T3 cells, ± 10% FCS; Small (S) or large (L) normal oral cells, ± 1 ng/ml TGFβ.
[b]Status: P = proliferating cells; NP = nonproliferating cells.
[c]Mean value ± S.E. or 8, 3, and 7 experiments for A431, 3T3, and oral cells, respectively.
[d]Not detectable.

TABLE 3. Fluorescence Analysis of Excitation Scan (λex 240–430 nm, λem 450 nm)†

Cell line	Media[b]	Status[c]	N[d]	Ratio[a] λem 450 nm	*P**
A431	–	P	8	1.51 ± 0.01	0.0009
A431	+	NP	8	1.31 ± 0.04	
3T3	+	P	10	1.57 ± 0.03	0.0003
3T3	–	NP	10	1.33 ± 0.04	
Oral cells	–	P	7	1.56 ± 0.02	0.0001
Oral cells	+	NP	7	1.42 ± 0.02	

†Three day control vs. treated cells were trypsinized and suspended within a fibrin clot and scanned as described.
[a]The ratio generated from two points on the scans, mean ± S.E.
[b]Media additives for A431, ± 100 ng/ml EGF; 3T3, ± 10% FCS; oral cells, ± 1 ng/ml TGFβ.
[c]Status: P = proliferating cells; NP = nonproliferating cells.
[d]Number of experiments.
*Differences in ratios between control and treated samples were analyzed by the two-sample *t*-test.

Fluorescence Analysis

Six excitation and five emission scans were used to analyze the cells in this study (Table 1). Data was generated from the scans by computing the ratio of relative intensities of the primary peak to points on the slopes for each of the designate excitation and emission scans. Several excitation scans demonstrated identifiable differences between proliferating vs. more slowly proliferating cells. These differences were noted for all three cell culture systems. While other excitation scans gave statistically significant results, the data obtained with the excitation scan (λex 240–430 nm, λem 450 nm) is being used as representative. Presentation of excitation scan data will be limited to this scan. A difference between growth-inhibited cells and control cells was seen in the A431 and oral cell culture systems with the emission scans (λex 340 nm, λem 360–660 nm), but this difference was not observed in the 3T3 system. No apparent differences were found in the remaining evaluated emission scans.

The excitation scan (λex 240–430 nm, λem 450 nm) had a broad peak between 320–350 nm (Fig. 5A–C). For purposes of data analysis, a ratio of the primary peak to a point on the down-slope of the curve at 370 nm was used. Representative normalized (λex 240–430 nm, λem 450 nm) scans for A431 cells are shown in Figure 5A. A comparison of the ratios between control (proliferating cells) and EGF treated A431 cells (nonproliferating cells) from eight separate experiments was

performed and analyzed using the two-sample *t*-test. The two cells population were significantly different with the more rapidly growing cells having the greater scan ratio ($P = 0.0009$, Table 3).

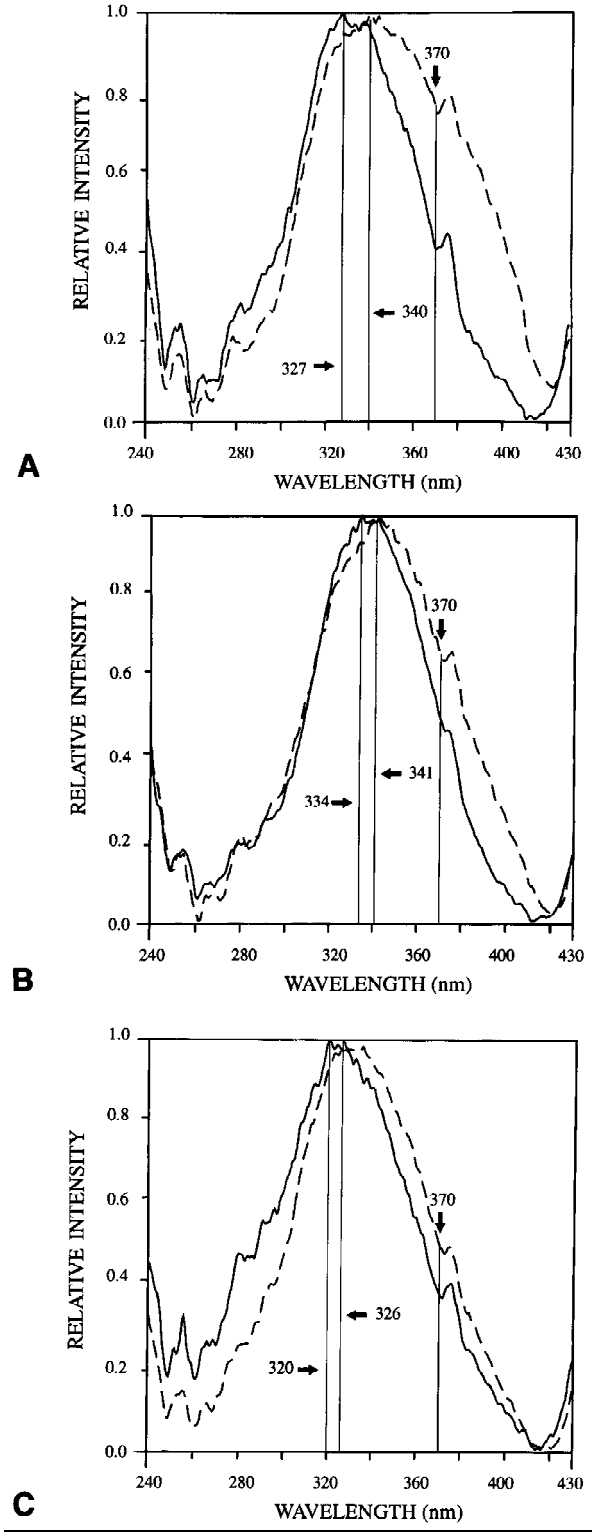

Similar analyses were used with the serum modulated 3T3 cells and the TGFβ treated oral cells. Analysis of 10 3T3 and seven oral epithelial experiments, demonstrated that the more rapidly-growing cells have a higher ratio than their matched slower growing cells: control 3T3 cells (10% serum, proliferating cells) vs. growth inhibited 3T3 cells (serum-free, nonproliferating cells) ($P = 0.0003$; Fig. 5B, Table 3); control oral epithelial cells (proliferating cells) vs. TGFβ treated oral cells (nonproliferating cells) ($P = 0.0001$; Fig. 5C, Table 3). A scatter plot of the ratios developed for the three cell systems is seen in Figure 6A-C. As seen in Figure 6A,C the EGF and control cells and the TGFβ and control cells show no overlap of their ratios. However, as seen in figure 6B, the 3T3 cell system has two ratio points denoted by arrows that do show an overlap.

In contrast to the excitation scans, a point on the curve up-slope at (415 nm) of the emission scan (λex 340 nm, λem 360–660 nm) was used to make a ratio with the main broad peak (439 nm) (Fig. 7). Using a comparison of these ratios, the more rapidly proliferating cells consistently demonstrated a greater ratio than the EGF treated, nonproliferating, slower growing cells (Table 4, Fig. 7). These differences reached statistical significance with the proliferating and nonproliferating A431 cells and oral cells, but not with the proliferating and nonproliferating 3T3 cells.

In fluorescence scans, the peaks are usually very broad. It is of note that the excitation scans (λex 240–430 nm, λem 450 nm) have sharp peaks at 375 nm and the emission scans at 409 nm. These two peaks were found to be the result of diffraction grating "ghosts." They could be determined for the emission scans by multiplying the excitation wavelength by 6/5, 9/5, or 3/2 and for the excitation scans by multiplying the emission wavelength by 5/6, 5/9, or 2/3. Thus, in the excitation scan (λex 240–430 nm, λem 450 nm), the 450 nm emission wavelength multiplied by 5/6 gives the ghost at 375 nm. In the emission scan (λex 340 nm, λem 360–660 nm), the sharp peak at

Fig. 5. Representative normalized excitation scans (λex 240-430 nm, λem 450 nm) of control (solid line) and treated (dotted line) (**A**) A431 cells; (**B**) 3T3 fibroblasts; and (**C**) normal oral epithelial cells. The (λex 240–430 nm, λem 450 nm) scans revealed consistent differences between inhibited and more rapidly growing cells for each cell type. Numbered vertical lines indicate wavelengths used to generate ratios in Table 3.

TABLE 4. Fluorescence Analysis of Emission Scan (λex 340 nm, λem 360–660 nm)[†]

Cell line	Media[b]	Status[c]	N[d]	Ratio[a] λex 340 nm	*P**
A431	–	P	7	1.19 ± 0.015	0.0001
A431	+	NP	7	1.03 ± 0.019	
3T3	+	P	10	1.23 ± 0.026	0.56
3T3	–	NP	10	1.12 ± 0.023	
Oral cells	–	P	7	1.19 ± 0.054	0.023
Oral cells	+	NP	7	1.16 ± 0.026	

[†]Three day control and treated cells were trypsinized and suspended within a fibrin clot and scanned as described.
[a]The ratio generated from two points on the scans, mean ± S.E.
[b]Media additives for A431, ± 100 ng/ml EGF; 3T3, ± 10% FCS; oral cells, ± 1 ng/ml TGFβ.
[c]Status: P = proliferating cells; NP = nonproliferating cells.
[d]Number of experiments.
*Differences in ratios between control and treated samples were analyzed by the two-sample *t*-test.

409 nm is the result of a grating ghost (6/5 multiplied by the excitation wavelength 340 nm). The xenon-arc lamp used in the spectrophotometer can give sharp lines at 422, 447, 460, 484, 495, 506, 521, and 529 nm. However, these lines were very weak and did not present a problem in the scans discussed.

DISCUSSION

A unique set of spectral features has been identified which characterized in vitro states of cellular proliferation. Through analyses based on ratios of points on the curves, a consistent excitation and emission spectral scan was identified which could distinguish rapid, proliferating cells from slow growing or nonproliferating cells. These scans were able to discriminate proliferation in three model systems in which the proliferative state was modulated by different methods. A431 epidermoid carcinoma cells were growth inhibited by exposure to EGF (100 ng/ml). Cell cycle analysis indicated a block in late S/G_2M which agrees with data from other cell systems [29,30]. The decrease in thymidine incorporation (Fig. 2) confirms that although the percentage of cells with an S-phase DNA content was not altered by EGF treatment (35 vs. 38% for control, Table 2), these are blocked non-replicating cells. 3T3 fibroblasts were growth inhibited in the presence of serum-free medium and cell cycle analysis showed the expected block in G0/G1 with a decrease in both S and G_2M cells. DNA synthesis was similarly inhibited. Normal oral epithelial cells were growth inhibited with TGFβ (1 ng/ml). Cell cycle analysis identified a TGFβ induction of a large cell population [see region 2 (R2), Figure 4B,F] that was predominantly in G0/G1. Whether these are just quiescent cells or ones now programmed towards terminal differentiation is at present unknown. In this respect, control cells also contain a population of large cells [region 2 (R2), Fig. 4A,E] which are blocked in G0/G1 and would represent cells that have left the cell cycle, are in a terminal differentiation pathway and now lack a proliferative capacity. These cells, however do not have the flattened morphology of terminally differentiated epithelial cells. Normal keratinocytes and oral cells generally have low cloning efficiencies with the majority of cells having limited proliferative capacity, i.e., in a terminal differentiation pathway. TGFβ has been shown to increase cell size but not differentiation of oral cells [31]. TGFβ-induced growth inhibition of oral and skin epithelial cells, under serum-free low calcium conditions, has been reported to be reversible, but our culture conditions and medium are different from these studies [32,33]. Although TGFβ induces differentiation of bronchial epithelial cells, the response of skin and oral keratinocytes to TGFβ depends on culture conditions, with growth inhibition being both reversible and irreversible, depending on calcium levels [33–35].

Normal oral epithelial cells show a much lower level of thymidine incorporation than the normal fibroblast cell line. This is probably based on their being a truly normal cell, whereas the 3T3 fibroblasts, although considered normal, have an increased life span and are probably im-

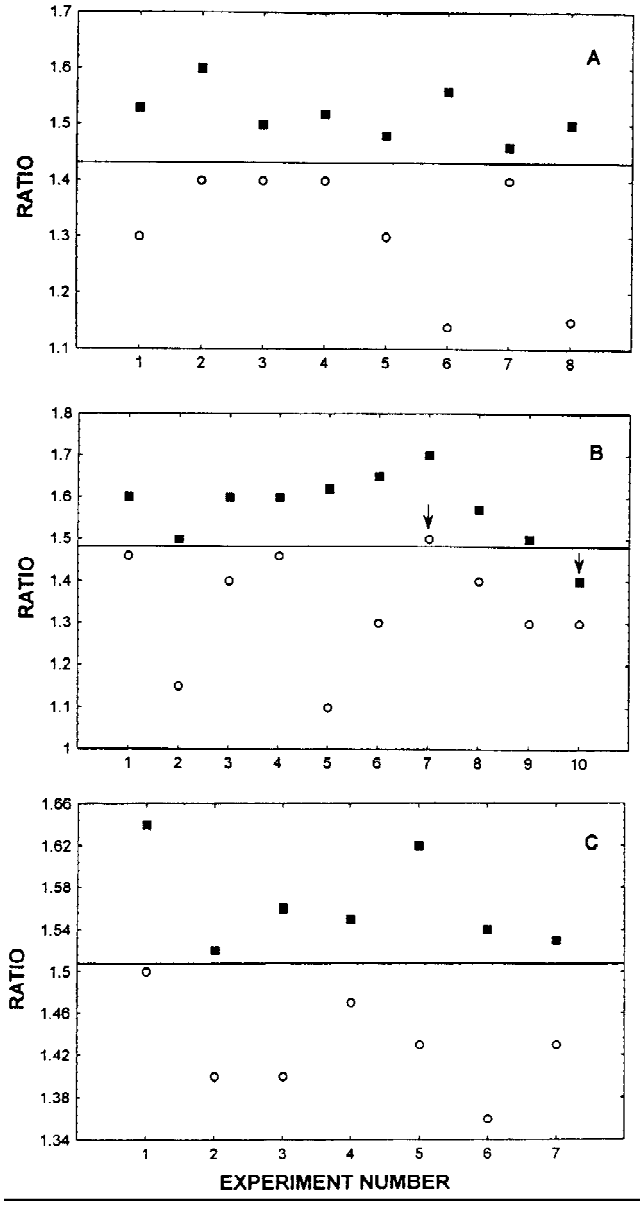

Fig. 6. This figure shows scatter graphs of the ratios determined for the proliferating and nonproliferating cells for the three cell systems studied. **A:** EGF-treated A431 cells (slow proliferation) vs. control A431 cells (rapid proliferation); **B:** serum starved 3T3 cells (slow proliferation) vs. 3T3 cells grown in 10% calf serum (rapid proliferation); and **C:** TGFβ-treated oral cells (slow proliferation) vs. control oral cells (rapid proliferation). The open circles represent ratios that were derived for those growth conditions used to produce slow proliferation and the closed squares represent those ratios developed for the conditions used to produce rapid cell proliferation.

mortal, although non-tumorigenic. Additionally, the normal cells have a lower S-phase fraction and contain a population of large cells (R2, Fig. 4) that are G0/G1 and non-proliferative.

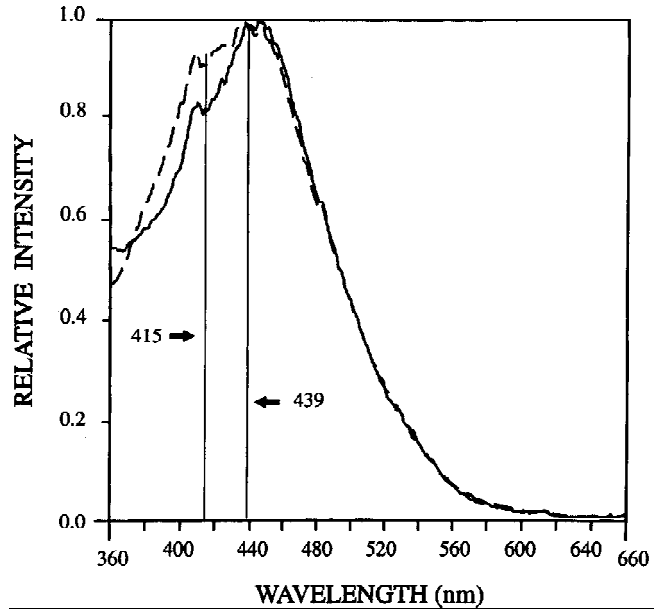

Fig. 7. Representative, normalized emission scans (λex 340 nm, λem 360–660 nm) of control (solid line) and EGF treated (broken line) A431 cells. Numbered vertical lines indicate wavelengths used to generate ratios in Table 4.

The biological basis of our study is that proliferation is a major phenotypic characteristic which distinguishes neoplastic from normal tissue and that fluorescence per unit area of tissue scanned should reflect these differences. In fact, the ratios generated from the excitation spectra (λex 240–430 nm, λem 450 nm) consistently discriminated proliferating from growth inhibited, nonproliferating cells. The change in spectral characteristics was nearly identical in each of three systems and was independent of whether cells were neoplastic or normal. The emission scan (λem 360–660, λex 340 nm) used in this study is comparable to the ones used by other researchers (discussed above) and discriminated proliferation in the A431 and and normal epithelial systems, but not the 3T3 cell system. The emission scan (λex 340 nm, λem 360–660 nm) may simply be less sensitive to changes in the 3T3 cell populations, or may be related to the place in the cell cycle where the cells become arrested.

The fluorescence patterns observed in the multiple scans performed in this study represent the summation of the fluorescence intensities of many intrinsic cellular fluorophores. The fluorescence patterns will be dominated by those molecules which absorb and emit at the wavelengths covered by the emission and excitation scans used. The cell systems under study are growth arrested

through different mechanisms resulting in blockages at different stages of the cell cycle. These growth inhibited cells would be expected to have many biochemical differences but share the phenotype of population growth arrest. The profile which demonstrated the most consistent differences related to the excitation scan (λex 240–430 nm, λem 450 nm). In this later scan, the broad peak maxima was always greater in the more rapidly proliferating cells when ratioed to a point on the down-slope (370 nm). Based on fluorescence patterns of known molecules, the excitation scan (λex 240–430 nm, λem 450 nm) is dominated by NADH which has an emission maxima of 450 nm and excitation maxima of 340 nm [10,36,37]. Both NADH and FAD fluorescence levels within cells are dependent on the presence of oxygen. Chance et al. have shown that changes in the relative amounts of oxygen in cell systems will be reflected in altered levels of NADH and FAD fluorescence, often within two to three minutes [36,37]. Gosalvez et al. have also shown that within tumor tissue slices there are different levels of NADH fluorescence at different locations either near or distant to blood vessels. This was thought to be reflective of the oxidation or reduction state of oxygenation of the tissue NAD/NADH at the location scanned [38]. In the systems employed in this study, a minimum of 20 minutes was needed to prepare the cell clots for spectral examination. During clot formation, the cells were kept in the same air environment used to generate the treatment conditions (5% CO_2 in air), and one would assume that by the time the clots were scanned, they had equilibrated to ambient air conditions. Once established, this equilibrium lasted for as long as 2 hours without changes in the scan patterns or ratios generated from them. Since the oxygen concentration was the same in the CO_2 incubator as in ambient air, we conclude that relative oxygen content is not a determinant of the observed results. Differences in the excitation scan (λex 240–430 nm, λem 450 nm) could, however, be interpreted as an overall increase in NAD in the slower growing cells as opposed to the faster proliferating cells [39]. Biochemical studies of cell extracts, from the three cell models of slow and rapidly proliferating cells used in this study, are currently underway to specifically identify levels of NAD/NADH and FAD/FADH.

The scans with the most discriminatory capacity in this study were excitation scans and not emission scans; the latter characteristically have been used to date by other researchers employing laser excitation. While lasers can generate more light energy, they are restricted to a single excitation wavelength. For identification of those molecules responsible for the differences seen among normal, preneoplastic and tumor cells, an instrument that can identify both emission and excitation maxima is advantageous. Clearly, an excitation scan that identifies a molecule whose fluorescence is lost or gained should have a confirmatory emission scan that shows a similar change. In fact, this was the case in our NMBA animal model, where the loss of collagen signal was verified by the loss of signal at 390 nm in the emission scan (λex 340 nm, λem 360–660 nm) and a concomitant loss of signal at 330 nm in the excitation scan (λex 200–360 nm, λem 380 nm) [17]. Both the emission maxima and excitation maxima matched those of collagen. The discriminatory excitation scans used in this study may represent another set of scans that can be added to the list of those used in the development of optical imaging of tumors. The best imaging systems may have to rely on both multiple emission and excitation scans for optimal resolution of tumor.

In summary, native tissue fluorescence is being investigated as a potential intermediate endpoint biomarker. In the present study, correlations between tissue autofluorescence and cellular proliferation have been identified. The establishment of non-invasive methods which reflect altered proliferation, a major characteristic of premalignant tissue, supports our aim in developing this technology.

ACKNOWLEDGMENTS

This work was supported in part by grants CA29502 from the NIH and 49547-C from NASA.

REFERENCES

1. Schantz SP, Alfano RR. Tissue autofluorescence as an intermediate endpoint in cancer chemoprevention trials. J Cell Biochem 1993; 17F:199–204.
2. Alfano RR, Tata DB, Cordero J, Tomashefsky P, Longo F, Alfano M. Laser induced fluorescence spectroscopy from native cancerous and normal tissue. IEEE J Quant Electr 1984; QE-20:1502–1511.
3. Alfano RR, Tang GC, Pradhan A, Lam W, Choy DSJ, Opher E. Fluorescence spectra from cancerous and normal breast and lung tissues. IEEE J Quant Electr 1987; QE-23:1806–1811.
4. Lam S, MacAulay C, Hung J, LeRichie J, Profio AE, Palcic B. Detection of dysplasia and carcinoma in situ with a lung imaging fluorescence endoscope device. J Thorac Cardiovasc Surg 1993; 105:1035–1040.

5. Cothren RM, Richards-Kortum R, Sivak M, Fitzmaurice M, Rava RP, Boyce GA, Doxtader M, Blackman R, Ivanc TB, Hayes GB, Feld MS, Petras RE. Gastrointestinal tissue diagnosis by laser-induced fluorescence spectroscopy at endoscopy. Gastrointest Endosc 1990; 36:105–111.
6. Schomacker KT, Frisoli JK, Compton CC, Flotte TJ, Richter JM, Nishioka NS, Deutsch TF. Ultraviolet laser-induced fluorescence of colon tissue: basic biology and diagnostic potential. Lasers Surg Med 1992; 12:63–78.
7. Schomacker KT, Frisoli JK, Compton CC, Flotte TJ, Richter JM, Deutsch TF, Nishioka NS. Ultraviolet laser induced fluorescence of colonic polyps. Gastroenterology 1992; 102:1155–1160.
8. Kapadia CR, Cutruzzola FW, Obrien KM, Stetz ML, Enriquez R, Deckelbaum LI. Laser induced fluorescence spectroscopy on human colonic mucosa. Gastroenterology 1990; 99:150–157.
9. Leffell DJ, Stetz ML, Milstone LM, Deckelbaum LI. In vivo fluorescence of human skin. Arch Dermatol 1988; 124:1514–1518.
10. Ince C, Ashruf JF, Sanderse EA, Pierik EG, Coremans JM, Bruining HA. In vivo NADH and Pd-porphyrin video fluoriphosphorimetry. In: Erdman W, Bruley DF, eds. "Advances in Experimental Medicine and Biology," Vol XIV. New York: Plenum Press, 1992, pp 267–275.
11. Alfano RR, Predhan A, Tang GC. Optical spectroscopic diagnosis of cancer and normal breast tissues. J Opt Soc Am [B] 1989; 6:1015–1023.
12. Das BB, Glassman WS, Alfano RR, Cleary J, Prudente R, Celmer E, Lubicz S. UV fluorescence spectroscopic technique in the diagnosis of breast, ovarian, uterus and cervix cancer. SPIE 1991; 1427:368–373.
13. Ramanujam N, Mitchell MF, Mahadevan A, Thomsen S, Silva E, Richards-Kortum R. Fluorescence spectroscopy: a diagnostic tool for cervical intraepithelial neoplasia (CIN). Gynecol Oncol 1994; 52:31–38.
14. Eng J, Lynch RM, Balaban RS. Nicotinamide adenine dinucleotide fluorescence spectroscopy and imaging of isolated cardiac myocytes. Biophys J 1989; 55:621–630.
15. Undenfriend S. "Fluorescence Assays in Biology and Medicine," Vol. 1. New York: Academic Press, 1962.
16. Undenfriend S. "Fluorescence Assays in Biology and Medicine," Vol. 2. New York: Academic Press, 1969.
17. Glasgold R, Glasgold M, Savage H, Pinto J, Alfano R, Schantz S. Tissue autofluorescence as an intermediate endpoint in NMBA-induced esophageal carcinogenesis. Cancer Lett 1994; 85:223–232.
18. Silberberg MB, Savage HE, Tang GC, Sacks PG, Alfano RR, Schantz SP. Detecting retinoic acid-induced biochemical alteration in squamous cell carcinoma using intrinsic fluorescence spectroscopy. Laryngoscope 1994; 104:278–282.
19. Sacks PG, Oke V, Vasey T, Lotan R. Retinoic acid inhibition of a head and neck multicellular tumor spheroid model. Head Neck 1989; 11:219–225.
20. Sacks PG, Oke V, Amos B, Vasey T, Lotan R. Modulation of growth, differentiation and glycoprotein synthesis by β-all-trans retinoic acid in a multicellular tumor spheroid model for squamous carcinoma of the head and neck. Int J Cancer 1989; 44:926–933.
21. Cohen SM, Purtilo DT, Ellwein LB. Pivotal role of increased cell proliferation in human carcinogenesis. Mod Pathol 1991; 4:371–382.
22. Shin DM, Voravud N, Ro JY, Lee LS, Hong WK, Hittelman WN. Sequential increase in proliferating cell nuclear antigen expression in head and neck tumorigenesis: a potential biomarker. J Natl Cancer Inst 1993; 85:971–978.
23. Lipkin M. Gastrointestinal cancer: pathogenesis, risk factors and the development of intermediate biomarkers for chemoprevention studies. J Cell Biochem 1992; 16G: 1–13.
24. Kamata N, Chida K, Kikimaru K, Horikoshi M, Enomoto S, Kuroki T. Growth-inhibitory effects of epidermal growth factor and overexpression of its receptors on human squamous cell carcinomas in culture. Cancer Res 1986; 46:1648–1653.
25. Zetterberg A, Larsson O. Kinetic analysis of regulatory events in G1 leading to proliferation or quisence of Swiss 3T3 cells. Proc Natl Acad Sci USA 1985; 82:5365–5369.
26. Kasperbauer JL, Neel HB III, Scott RE. Proliferation and differentiation characteristics of normal human squamous mucosal cells of the upper aerodigestive tract. Ann Otol Rhinol Laryngol 1990; 99:29–37.
27. Fingert HJ, Chen Z, Mizrahi N, Gajewski WH, Bamberg MP, Kradin RL. Rapid growth of human cancer cells in a mouse model with fibrin clot subrenal capsule assay. Cancer Res 1987; 47:3824–3829.
28. Alfano RR, Pradhan A, Tang GC, Das K, Yoo M. Optical spectroscopy may offer novel diagnostic approaches for the medical profession. In: Goldman L, ed. "Laser Non-Surgical Medicine." Lancaster, PA: Technomic Publishing Co., 1991, pp 79–80.
29. Laderoute KR, Ausserer WA, Knapp AM, Grant TD, Sutherland RM. Epidermal growth factor modified cell cycle control in A431 human squamous carcinoma cells damaged by ionizing radiation. Cancer Res 1994; 54: 1407–1411.
30. Vivien D, Galera P, Lebrun E, Loyau G, Pujol JP. Differential effects of transforming growth factor-β and epidermal growth factor on the cell cycle of cultured rabbit articular chondrocytes. J Cell Physiol 1990; 143:534–545.
31. Sundqvist K, Lliu Y, Arvidson K, Ormstad K, Nilsson L, Toftgard R, Grafstrom RC. Growth regulation of serum-free cultures of epithelial cells from normal human buccal mucosa. In Vitro Cell Dev Biol 1991; 27A:562–568.
32. Shipley GD, Pittelkow MR, Wille JJ Jr, Scott RW, Moses HL. Reversible inhibition of normal human prokeratinocyte proliferation by TGFβ transforming growth factor-growth inhibitor in serum-free medium. Cancer Res 1986; 46:2068–2071.
33. Kasperbauer JL, Neel HB, Scott RE. Proliferation and differentiation characteristics of normal human squamous mucosal cells of the upper aerodigestive tract. Ann Otol Rhinol Laryngol 1990; 99:29–37.
34. Masui T, Wakefield LM, Lechner MA, Sporn MB, Harris CC. Type beta transforming growth factor is the primary differentiation-inducing serum factor for normal human bronchial epithelial cells. Proc Natl Acad Sci USA 1986; 83:2438–2442.
35. Matsumoto K, Hashimot K, Hashiro M, Yoshimasa H, Yoshikawa K. Modulation of growth and differentiation in normal human keratinocytes by transforming growth factor-β. J Cell Physiol 1990; 145:95–101.
36. Chance B, Schoener B, Oshino R, Itshak F, Nakase Y. Oxidation-reduction ratio studies of mitochondria in freeze-trapped samples. NADH flavoprotein fluorescent signals. J Biol Chem 1979; 254:4764–4771.

37. Chance B, Cohen P, Jobis F, Schoener B. Intracellular oxidation-reduction rates in vivo. The microfluorometry of pyridine nucleotide gives a continuous measure of the oxidation state. Science 1962; 137:499–508.
38. Gosalvez M, Thurman RG, Chance B, Reinhold HS. Indication of hypoxic areas in tumors from in vivo NADH fluorescence. Eur J Cancer 1972; 8:267–269.
39. Jacobson EL, Jacobson MK. Pyridine nucleotide levels as a function of growth in normal and transformed 3T3 cells. Arch Biochem Biophys 1976; 627–634.